CHAPTER IV

Low-powered programmable beam steering in patch antenna array

4.1. INTRODUCTION

The need of today's radar systems is precise, real-time and fast tracking of moving targets and hence, quick steering of beam is desirable. Fast beam steering is realized electronically in phase array antenna using T/R modules which comes with their distinct disadvantages of beign expensive, bulky and with high power consumption [1-3]. Metasurface superstrate (MS) techniques for steering the beam, as mentioned in Chapter I, have some distinct advantages, where the parent design of the antenna is not to be altered post fabrication. The reported literatures [4-9] mention using PIN diodes, mechanical actuators and fluidic controls in metasurface for scanning the beam. A large number, precisely 72 PIN diodes, have been incorporated in MS to achieve beam scanning in [4], while the other two techniques are slow and bulky. It needs to be mentioned here that the MS techniques have only been tested for a single antenna system.

In this chapter, impetus have been given to develop an electronically programable metasurface superstrate (MS) based beam steering technique for an array system. Less number of PIN diodes are strategically placed in MS to reduce the biasing complexity. Beam steering is first tested by placing MS over a single patch antenna and then verified for a 1×4 patch antenna array by changing the state of the PIN diodes. All the simulations are carried out using CST microwave studio.

4.2. DESIGN AND SIMULATION

4.2.1. Metasurface unit cell

The proposed phase reconfigurable metasurface unit cell, in the front side has a square ring with two metal strips of unequal widths placed vertically and horizontally crossing each other at the mid point. The vertical strip is connected with the square loop as shown in Figure 4.1(a). The back consists of a metal strip and a centrally aligned metal rectangle between which a PIN diode is placed. Schematic is given in Figure 4.1(b). The mentioned PIN diode placement in the unit cell reduces the biasing complexities when making it into a larger arrangement. The ON state of PIN diode is modelled as a R-L-C series circuit in simulation. A metalized via is connected through the top and bottom surface at the center of the unit cell as shown in Figure 4.1(c). The unit cell is designed on a 1.27mm thick Rogers 5880LZ substrate with $\varepsilon_r = 2.2$ and $\tan\delta = 0.0021$. The periodicity of the

metasurface unit cell in *x* and *y* direction is kept as $L = W = 10mm$, which is $< \frac{\lambda o}{2}$ at 10GHz. The dimensions the MS unit cell in written in Table 4.1.

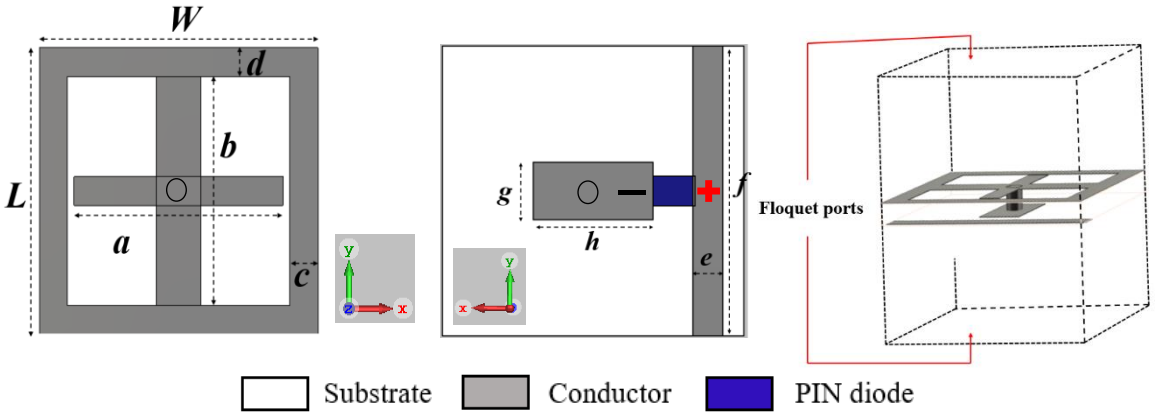

(a) (b) (c)

Figure 4.1. Unit cell design- (a) front view, (b) back view showing the position of PIN diode (anode and cathode indicated by "+" and "–" signs, respectively) and (c) Floquet ports configuration.

Table 4.1 Optimized parameter of metasurface unit cell

Parameters	***L***	***W***	***a***	***b***	***c***	***d***	***e***	***f***	***g***	***h***
Dimension (mm)	10	10	7.4	8	1	1	1	10	2	4

The transmission characteristics of the MS is evaluated by simulation using CST Microwave Studio. Frequency domain solver is used where the periodic boundary conditions are applied in *x* and *y* directions and placed such that EM wave propagates in ± *z*-direction, refer Figure 4.1(c). The PIN diode SMP1320-079LF is modelled as a 0.75 Ω resistor in the ON state and as a parallel combination of a 0.23 pF capacitor and a 3 kΩ resistor in the OFF state. The values are taken from the data sheet attached as Appendix 1. Two transmission states are obtained with the PIN diode in ON and OFF state. The transmission amplitudes and phase for the two modes are indicated in Figure 4.2(a). Both the modes show a -3dB pass band in the frequency range of 8.6 – 10.6 GHz. At 10GHz, the difference in transmission amplitude is only 0.8dB between the two modes. This validates that the designed metasurface can transmit the incoming wave in both ON and OFF state. A lag in the transmission phase of 33° in ON state is also observed.

The simulated surface current densities for the OFF and ON states of the PIN diodes for top and bottom surface of the metasurface unit cell is drawn in Figure 4.2(b) and (c), respectively. The current intensity changes on the surface of the metasurface unit cell for both the operating states. In the OFF state, the surface current vectors are uniformly distributed over the metal strip, however, in the ON state it is mainly concentrated to one half of the structure. The current paths for the two states are opposite. This variation in distribution of current density indicates the transmission phase shift.

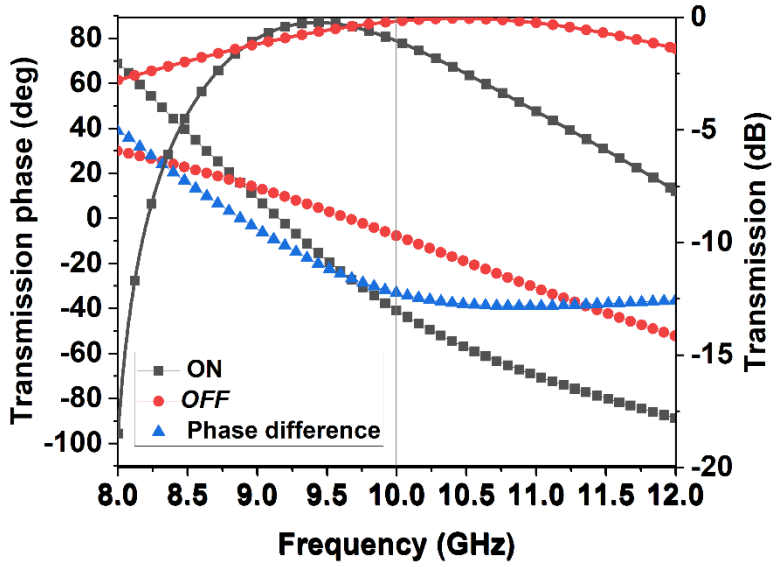

(a)

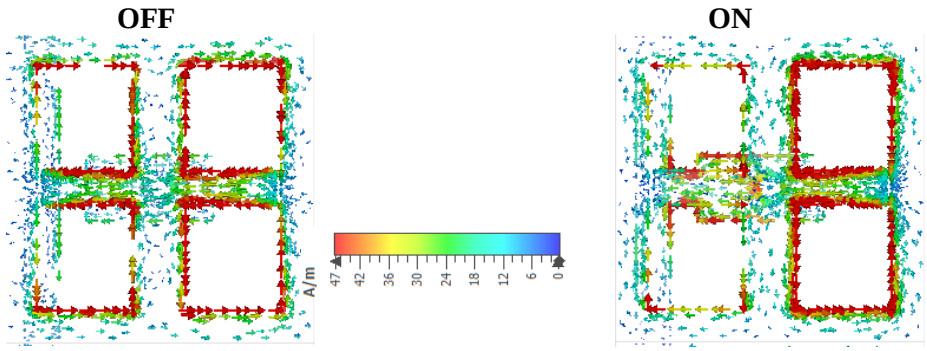

(b)

Figure 4.2 (a) Transmission amplitude and phase of the metasurface unit cell for PIN diodes in ON and OFF state and relative phase difference, (b) simulated surface current distribution of the metasurface unit cell

4.2.2. Single antenna with metasurface superstrate (MS)

First a single patch is designed at 10GHz. The design frequency 10GHz is chosen as the difference in transmission amplitude between the ON and OFF mode of MS is minimum, refer to Figure 4.2(a). Thereafter, the ability of the MS to steer the beam of single patch antenna is verified.

Single patch antenna

A single patch antenna is designed to resonate at 10GHz on a 1mm thick FR4 substrate with $\varepsilon_r = 4.3$ and $\tan\delta = 0.02$. The antenna is fed coaxially at a point of 50Ω impedance as illustrated in schematic in Figure 4.3. The dimension of the patch antenna is given in Table 4.2.

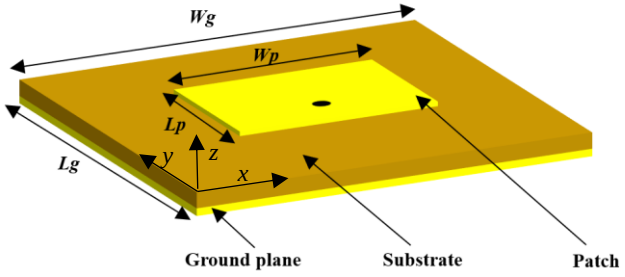

Figure 4.3 Schematic representation of patch antenna

Table 4.2 Design parameters of single patch antenna

Parameter	**Dimension (mm)**
Length of ground plane, L_g	25
Width of ground plane, W_g	25
Length of the patch, L_p	6.3
Width of the patch, W_p	9.3

Single patch antenna-metasurface assembly

The phase tunable metasurface superstrate (MS) is realized by making a 3×4 arrangement of the metasurface unit cell to cover the antenna completely. Each row consists of 3 PIN diodes making a total of 12 PIN diodes numbered as P1 to P12, as shown in Figure 4.4(a). One of the advantages of this design is that all the pin diodes of a row in x-direction can be controlled at a time using a single biasing line. The metasurface is placed as a superstrate

at an optimized distance, $h = 7.5mm$, above the patch antenna, which is $\sim\lambda o/4$, where λo is the free space wavelength at 10GHz. The schematic of the MS placed over the single patch antenna is shown in Figure 4.4(b). Beam tunability is observed by changing the states of PIN diodes. The ON state of the PIN diode is depicted as **1** while the OFF state as **0**. Three modes of operation is studied for the antenna-MS assembly as indicated in Table 4.3.

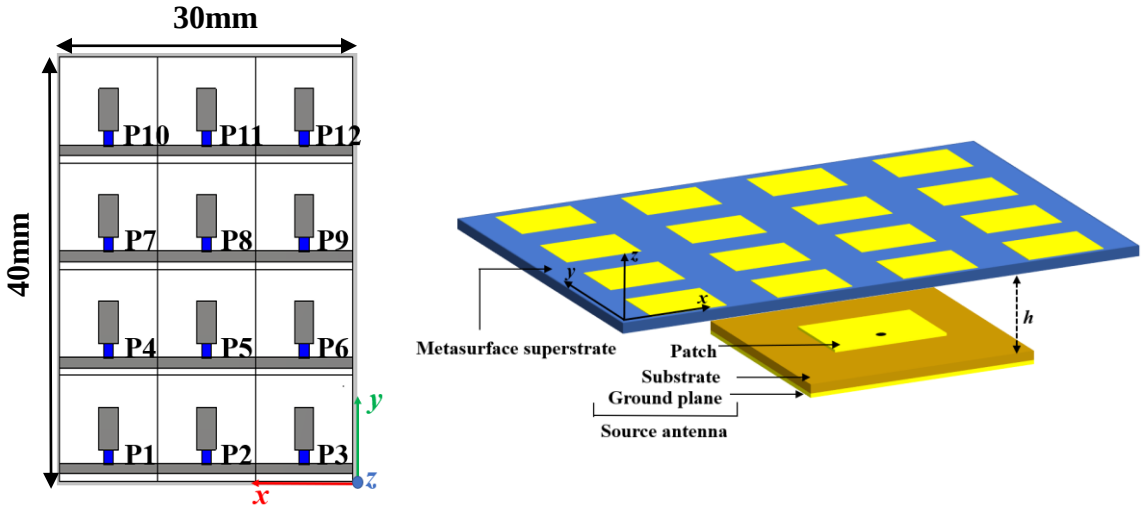

(a) (b)

Figure 4.4 (a) Bottom view of the metasurface with the PIN diodes, (b) schematic of the antenna with metasurface placed as a superstrate.

Table 4.3 Modes of operation of the PIN diodes

PIN diodes	**P1**	**P2**	**P3**	**P4**	**P5**	**P6**	**P7**	**P8**	**P9**	**P10**	**P11**	**P12**
Mode 1	0	0	0	0	0	0	0	0	0	0	0	0
Mode 2	0	0	0	0	0	0	1	1	1	1	1	1
Mode 3	1	1	1	1	1	1	0	0	0	0	0	0

Simulated results

The single antenna element is excited and the simulated return loss and radiation pattern for the antenna-MS assembly is studied for the three modes. The return loss plots in Figure 4.5(a) shows that resonance frequency shifts $\pm 60MHz$ on placing MS. The beam steering is realized by independently manipulating the states of the PIN diodes according to the modes described in Table 4.2. Figures 4.5(b and c) plots the radiation pattern of the single patch antenna with the MS in Modes 1,2 and 3 for $\phi = 0^{\circ}$ (*xz*-plane) and $\phi = 90^{\circ}$

(*yz*-plane). No significant change in the radiation pattern for all the three modes is observed from Figure 4.5(b). The proposed MS is able to steer the main beam to ±25° for ϕ = 90° plane as seen from Figure 4.5(c). In accordance with the phased array's operating principle, as given in refrence [10], the beam angles toward the direction where the phase lags. Here, since the ON state lags, (refer Figure 4.2(a)), it is possible to tilt the beam towards section of the MS where the PIN diodes are in ON state. The simulated performance of the antenna-metasurface assembly is written in Table 4.4.

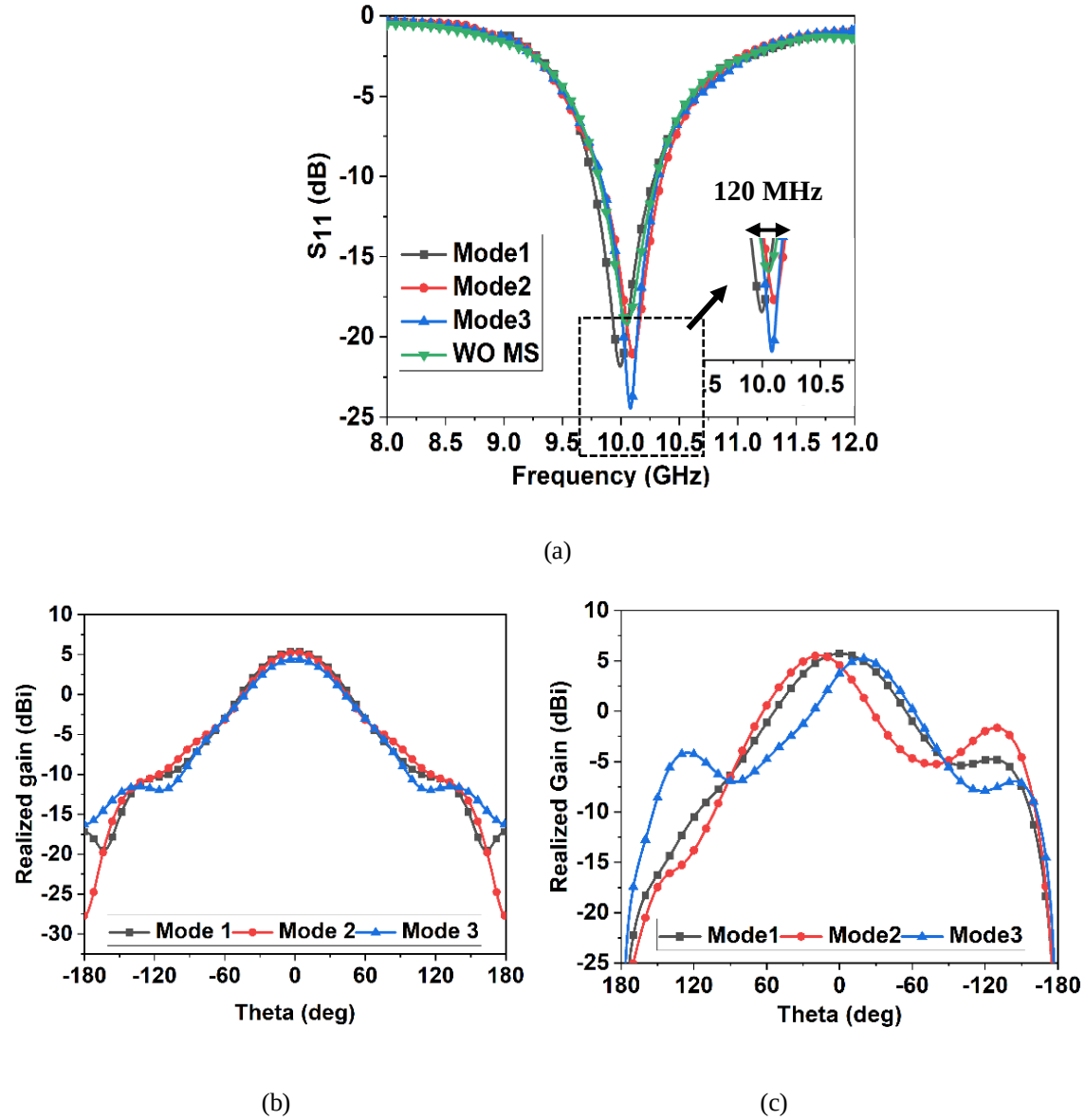

Figure 4.5 Simulated (a) return loss, S_{11} of the antenna without (WO) MS and with MS for three different modes. Simulated radiation pattern for three modes at (b) ϕ = 0° and (c) ϕ = 90°.

Table 4.3 Simulated performance of the single patch antenna-metasurface assembly at 10GHz

Modes	-10dB bandwidth (GHz)	$\phi = 0^{\circ}$		$\phi = 90^{\circ}$	
		Beam direction (deg)	Gain (dBi)	Beam direction (deg)	Gain (dBi)
Mode1	9.75-10.29	0	5.42	0	5.72
Mode2	9.8-10.35	0	5.21	25	6.46
Mode3	9.82-10.32	0	4.43	-27	6.65

4.2.3. 1 × 4 patch antenna array with metasurface superstrate (MS)

A 1 × 4 antenna array is designed by replicating the single patch antenna described in the above section. A total of 4 × 12 metasurface unit cells with 48 PIN diodes are arranged in so as the antenna array is fully covered. Figure 4.6(a) shows the schematic of placement of 1×4 antenna array with the MS. The height of the placement of MS is kept same as that in the case of single antenna i.e. $h = 7.5mm$. The top view of the 1×4 antenna array with MS is displayed in Figure 4.6(b), where, PIN diodes are represented by the blue bars. The three modes of operation for the 1×4 antenna array with MS is kept similar as single patch antenna as described in Table 4.2. Mode I indicates that all the PIN diodes are in the OFF state. In Mode II all the 24 PIN diodes on the upper half of the MS are in ON state, while rest of them are in OFF state, represented as red rectangle in Figure 4.6(b). A vice versa of the Mode II combination is done for the Mode III, where only the lower half is in ON state marked within the green rectangle in Figure 4.6(b). The dimension of the 1 × 4 antenna array-metasurface assembly is mentioned in Table 4.5.

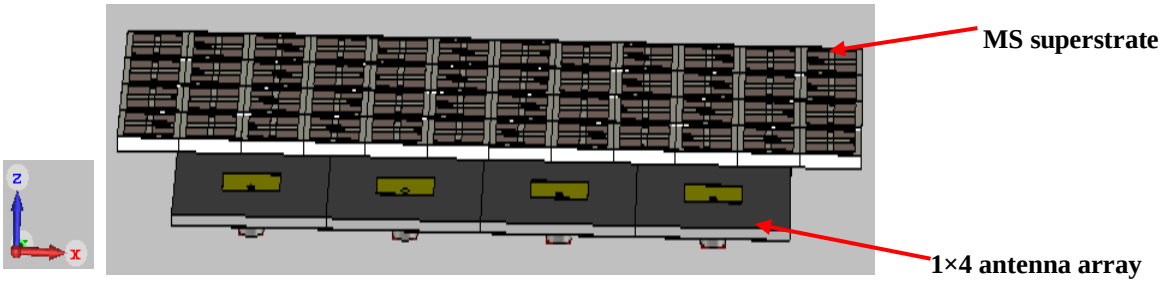

(a)

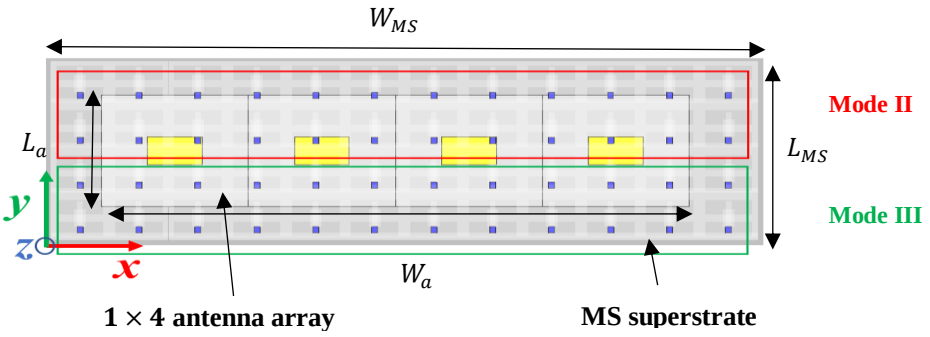

(b)

Figure 4.6 (a) Schematic of the metasurface superstrate with 1 × 4 antenna array and (b) the top view of antenna array indicating the positions of PIN diodes.

Table 4.5 Dimension of 1 × 4 antenna array-metasurface superstrate assembly

Parameters	Dimension (mm)
Length of the array, L_a	25
Width of the array, W_a	100
Length of the MS, L_{MS}	40
Width of the MS, W_{MS}	120

Simulated results

All the four elements of the 1×4 antenna array is excited simultaneously for the three different modes mentioned above. Figure 4.7(a-b) plots the radiation pattern of the 1×4 antenna array with MS for $\phi = 0°$ and $\phi = 90°$. Quantitative summary is tabulated in Table 4.6. A total scan volume of 47° is seen in $\phi = 90°$ for different modes of operation. No significant change in the radiation pattern takes place for $\phi = 0°$ plane. The 3-D radiation plot for three different modes at $\phi = 90°$ is shown in Figure 4.7(c).

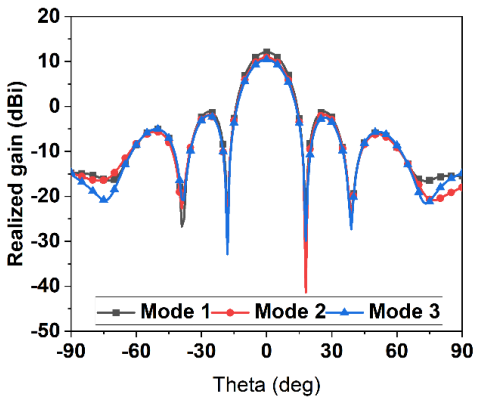

(a)

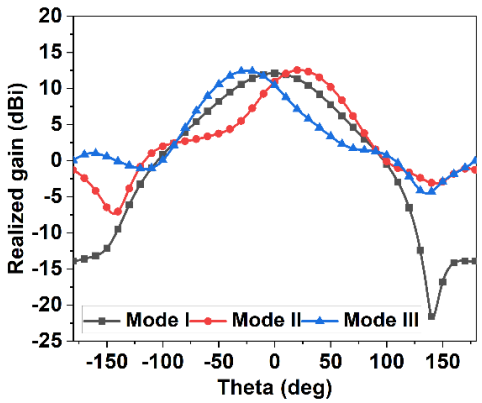

(b)

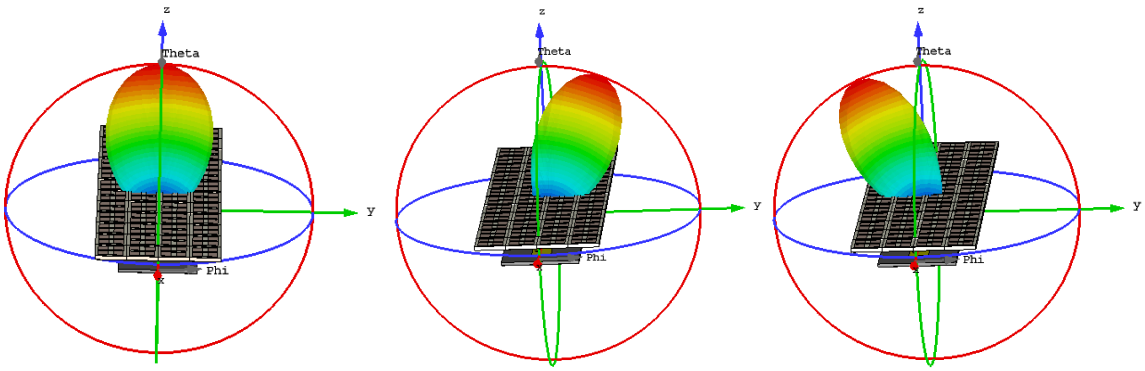

(c)

Figure 4.7 Simulated radiation pattern of the 1 × 4 antenna array – MS assembly for the three different modes of operation at (a) $\phi = 0°$ and (b) $\phi = 90°$. (c) 3-D radiation pattern plot for three different modes at $\phi = 90°$.

Table 4.6 Simulated performance of the 1 × 4 array-metasurface assembly

Modes	**-10dB bandwidth (GHz)**	**$\phi = 0^{\circ}$**		**$\phi = 90^{\circ}$**	
		Beam direction (deg)	**Gain (dBi)**	**Beam direction (deg)**	**Gain (dBi)**
Mode 1	9.75-10.32	0	12.1	0°	12.1
Mode 2	9.87-10.43	0	10.9	22°	12.5
Mode 3	9.87-10.41	0	10.4	-25°	12.5

4.3. IMPLEMENTATION AND MEASUREMENT

4.3.1 Single antenna-metasurface superstrate assembly

Fabrication

The metasurface superstrate (MS) is fabricated with the dimension given in Table 4.1. The biasing network schematic of the metasurface layer is illustrated in the Figures 4.8(a-b). The vias are modelled keeping in mind to reduce the biasing complexities when made into a larger arrangement of unit cell. The top layer of the MS is grounded completely with the help of the vias. This design also allows an extremely simple biasing as a single voltage can be applied at the edges of the MS surface to control all PIN diodes in a redundant topology, tolerant to faults and variations of the diode dc-resistance. RF inductor (Thin Film Inductor, 2.2 nH, MULTICOMP PRO) is used as RF choke. The top and bottom view of the fabricated MS is shown in Figures 4.8(c and d) respectively. The PIN attachement is given in the inset. The single patch antenna is fabricated using the dimensions given in Table 4.2. For placing the (MS) above the antenna, a 3D printed PLA stand is built, as shown in Figure 4.8(a).

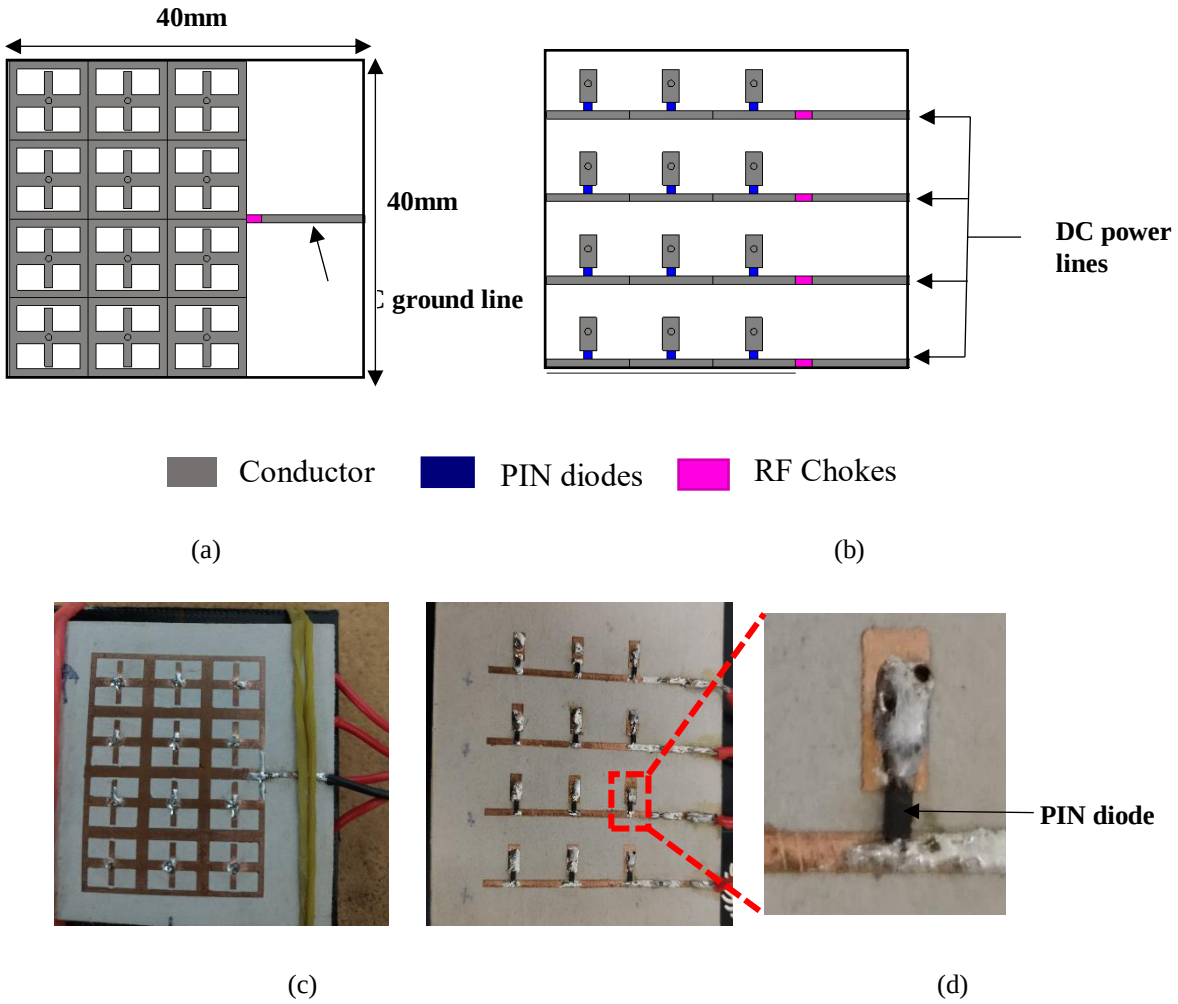

Figure 4.8 Schematic of the biasing network of the MS (a) top view and (b) bottom view. Fabricated MS with biasing lines (c) top view and (d) bottom view with inset showing PIN diodes attachment.

S_{11} *measurement*

Initially the single patch antenna is tested for its return loss, S_{11}, using vector network analyser as described in Chapter III. The measurement setup of single patch antenna is shown in Figure 4.9(a). The fabricated metasurface is placed as a superstrate above the antenna at a distance $h = 7.5mm$, and the return loss, S_{11} values for all the three modes are measured as shown in Figure 4.9(b). A 9V HW marked non-rechargeable battery is used to power the PIN diodes.

(a) (b)

Figure 4.9 Photograph of the S_{11} measurement setup with (a) single patch antenna and (b) single patch antenna-metasurface superstrate assembly.

Figure 4.10 illustrates the measured S_{11} for the single patch without (WO) and with (W) the MS for all the three modes of operation. The operational -10dB bandwidth of the single antenna remains almost constant with a marginal shift of $\Delta f = 90MHz$, in resonance frequency, as can be seen in the inset of Figure 4.10. This validates placement of the MS does not much change the performance of the antenna.

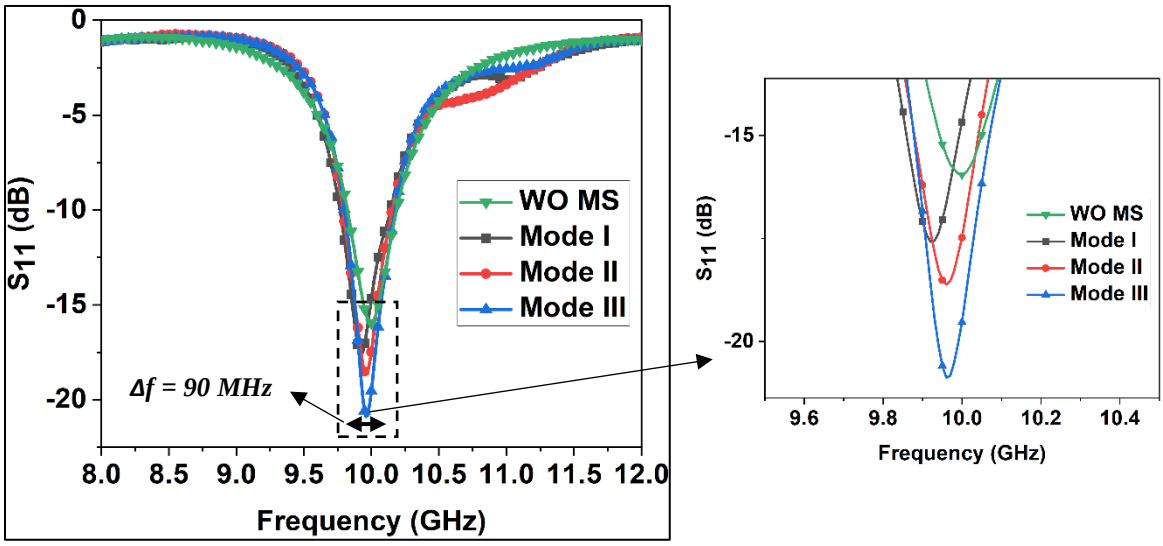

Figure 4.10 Measured S_{11} of the single patch antenna WO MS and with (W) MS for the three modes of operation of PIN diodes. Inset showing the expanded view of resonant frequency dip.

Radiation pattern measurement

Radiation pattern for single antenna with MS is measured using Diamond Engineering DAMS 6000 series measurement setup as discussed in Chapter III. The pattern is measured for both the orthogonal planes viz. $\phi = 0^{\circ}$ and $\phi = 90^{\circ}$. Figure 4.11(a) shows the measurement setup for the radiation pattern of single antenna.

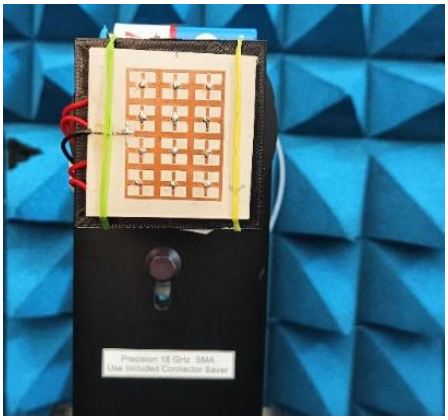

(a)

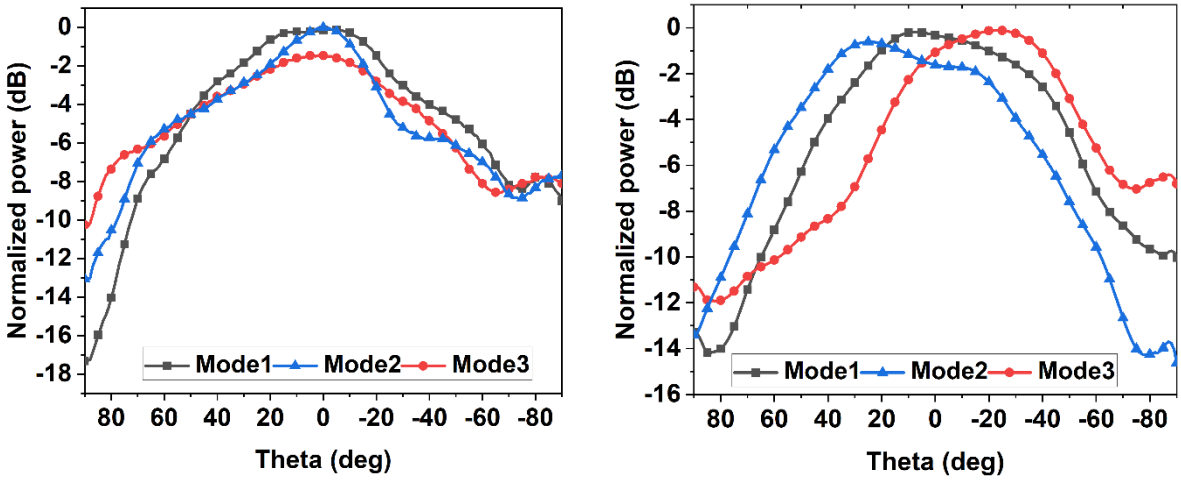

(b) (c)

Figure 4.11 (a) Radiation pattern measurement setup. Measured radiation pattern of single patch antenna with MS in (b) $\phi = 0^{\circ}$ and (b) $\phi = 90^{\circ}$planes.

4.3.2 1 × 4 antenna array-metasurface assembly

The 1 × 4 antenna array is fabricated using the dimension mentioned in Table 4.3. The antenna array is fixed to a 3D printed PLA stand to hold the metasurface superstrate as

shown in Figure 4.12(a). To completely cover the antenna array, a 12×4 arrangement of metasurface unit cell is fabricated along with the biasing lines. Figures 4.12 (b-c) show the top and bottom view of the fabricated metasurface array along with the biasing lines.

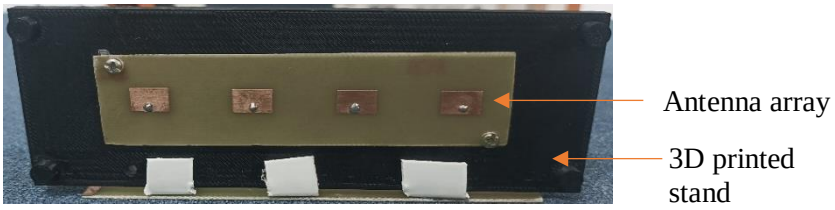

(a)

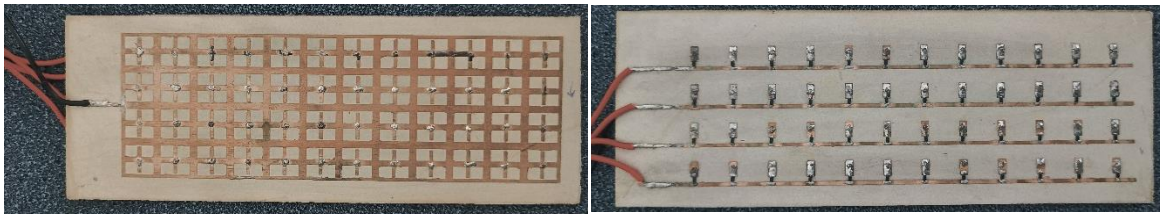

(b) (c)

Figure 4.12 Fabricated prototype of (a) 1×4 antenna array fixed in a 3D printed stand. A 12×4 metasurface layer (b) top view and (c) bottom view.

Radiation pattern measurement

The radiation pattern measurement is carried out in similar way as described in the previous section for unit patch antenna. All the antennas are simultaneously excited for getting a cummilative pattern of the 1×4 array. A 1:4 T-junction power divider is designed and fabricated. The output port of the power divider has an insertion loss of $\approx$ -8dB. The antennas are fed through the output port of the power divider using RG316 flexible Coaxial Cable (SMA M to SMA F). The setup for simultaneous excitation of the antenna array is shown in Figure 4.13(a). Figures 4.14(a-b) present the measured radiation patterns for different modes of excitation.

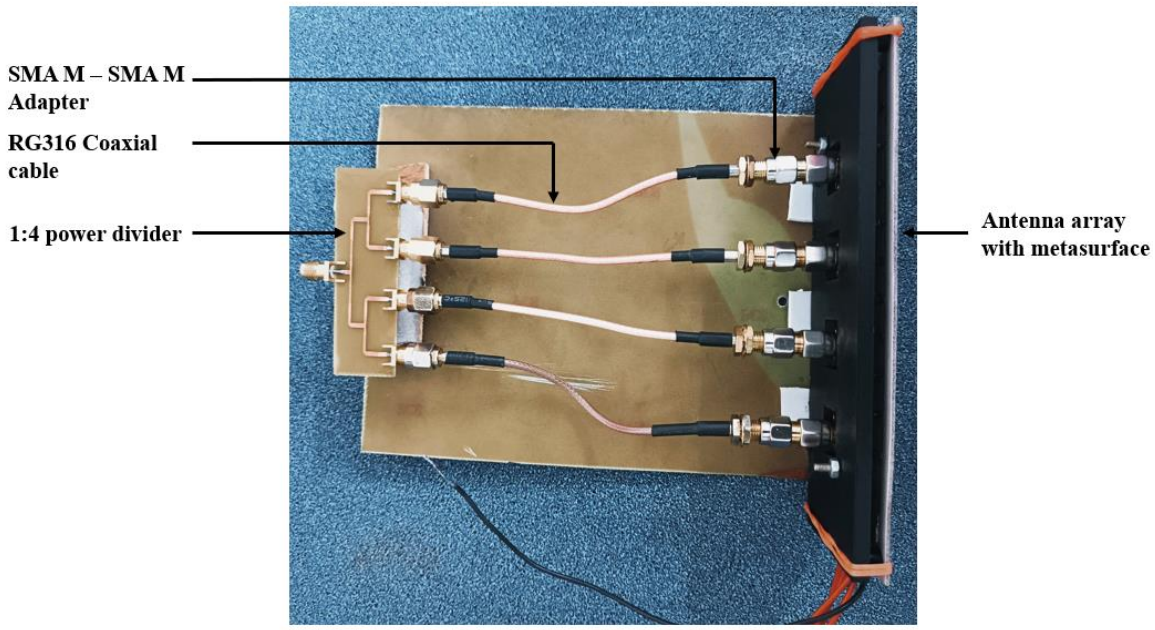

(a)

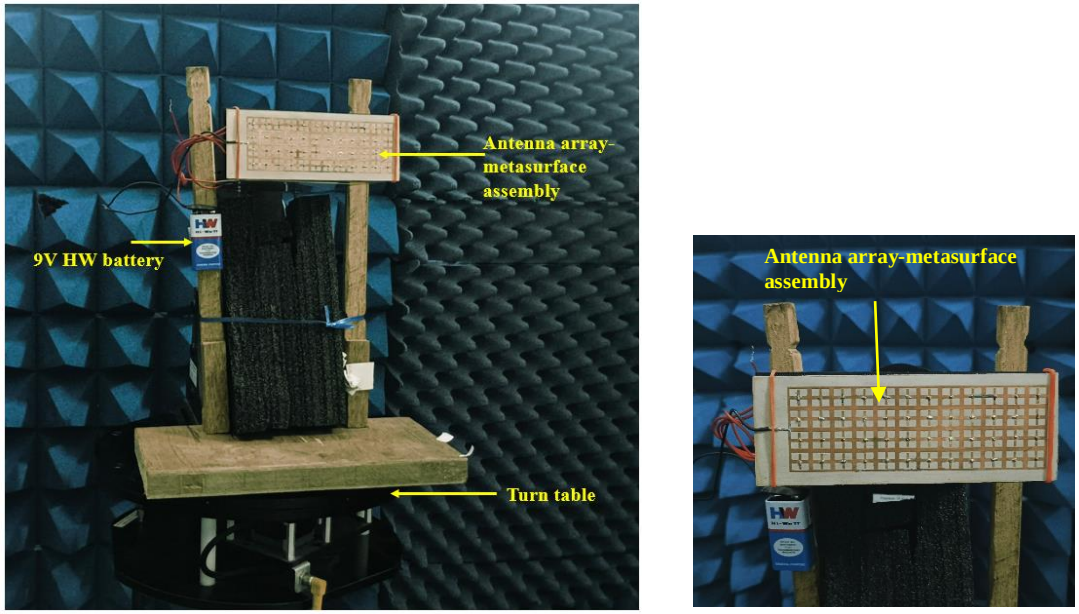

(b)

Figure 4.13 (a) Setup for simultaneous excitation of all the antenna elements of 1 × 4 array using 1:4 power divider. (b) Radiation pattern measurement setup of array-MS assembly.

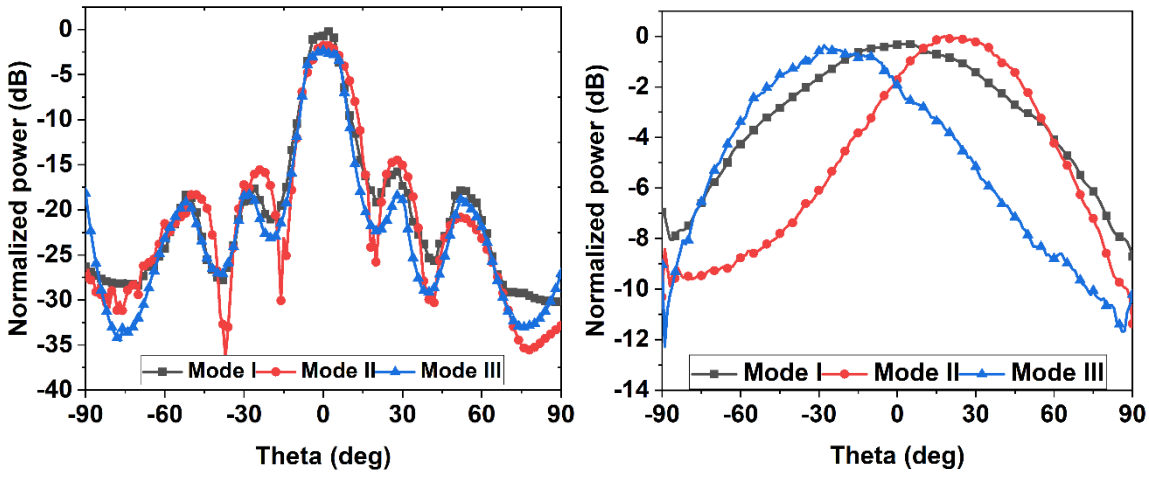

Figure 4.14 Measured radiation pattern of 1 × 4 antenna array-MS assembly in (a) $\phi = 0°$ and (b) $\phi = 90°$ planes.

Table 4.7 consolidates the scanning performance of the single and 1 × 4 antenna array-metasurface superstrate assembly.

Table 4.7 Quantatitive performance of the single and 1 × 4 antenna array-MS in terms of beam steering volume and gain.

Antenna type	**Maximum beam direction**				**Gain (dB)**	
	Simulated		**Measured**		**Simulated**	**Measured**
	$\boldsymbol{\phi = 0°}$	$\boldsymbol{\phi = 90°}$	$\boldsymbol{\phi = 0°}$	$\boldsymbol{\phi = 90°}$		
Single	0	±25°	0	±27°	7.46	7.19
1 × 4 *array*	0	±22°	0	±27°	12.5	10.3

In the 1×4 array configuration at $\phi = 0°$, a maximum sidelobe level (SLL) of -14.49 dB is observed in Mode II, while a minimum SLL of -18.33 dB is observed in Mode III. For $\phi = 90°$, the maximum SLL occurs in Mode I with a value of −7 dB, whereas the minimum SLL of -12 dB is observed in Mode III.

The simulated and measured reults are in close proximation.The variations in the scanning range and gain values could be attributed to the fact that the in simulation, boundary conditions are different as compared to practical measurement setup. Some fabrication tolerance could also contribute to the variation.

4.4. CHAPTER SUMMARY

The salient features of the work presented in this chapter are centered on a metasurface superstrate–based beam steering technique that is both low-power consuming and experimentally validated. The proposed metasurface unit cell exhibits a tunable transmission phase property, which is electrically controlled using a single PIN diode. The technique is initially demonstrated on a single patch antenna and subsequently extended to a 1×4 antenna array. For the single antenna case, only 12 PIN diodes are employed within the metasurface to achieve beam steering, representing just one-third of the number reported in [11]. Similarly, for the 1×4 antenna array, only 48 PIN diodes are required, which is two-thirds of the diode count used for a 1×2 array in [12]. The system achieves a total scan volume of 54° in both the single and 1×4 patch antenna array configurations. The unit cell design of the metasurface also allows for a simplified biasing network, enabling all diodes in a row to be controlled by a single voltage source. Importantly, the resonance frequency of the antenna remains unaffected by the integration of the metasurface superstrate, ensuring stable performance during beam steering.

References

[1]. Wenxing, Z., Qiang, W., & Shuwei, Z. Thermal design of T/R modules in airborne phased array antenna. *Conference (JIMEC 2017)*, 2017. Copyright © 2017.

[2]. Mass, J. D., S. R., & D. W. Overcoming planar phased array circuit design challenges. *Microwave Journal*, April 6, 2023. https://www.microwavejournal.com/articles/39773-overcoming-planar-phased-array-circuit-design-challenges

[3]. Rathod, S., Sreenivasulu, K., Beenamole, K., & Ray, K. Evolutionary trends in transmit/receive module for active phased array radars. *Defence Science Journal*, 68(6):553, 2018. DOI:10.14429/dsj.68.12628

[4]. Das, P., Mandal, K., & Lalbakhsh, A. Beam-steering of microstrip antenna using single-layer FSS based phase-shifting surface. *International Journal of RF and Microwave Computer-Aided Engineering*, 32(3), 2021. DOI:10.1002/mmce.23033

[5]. Verma, A., Arya, R. K., & Raghava, S. N. Metasurface superstrate beam steering antenna with AMC for 5G/WiMAX/WLAN applications. *Wireless Personal Communications*, 128(2):1153–1170, 2022. DOI:10.1007/s11277-022-09993-4

[6]. I. Russo, L. Boccia, G. Amendola, and G. Di Massa. Tunable pass-band FSS for beam steering applications. *Proceedings of the Fourth European Conference on Antennas and Propagation*, Barcelona, Spain, pp. 1–4, 2010.

[7]. L.-Y. Ji, Z.-Y. Zhang, and N.-W. Liu. A two-dimensional beam-steering partially reflective surface (PRS) antenna using a reconfigurable FSS structure. *IEEE Antennas and Wireless Propagation Letters*, 18(6):1076–1080, June 2019. DOI:10.1109/LAWP.2019.2907641

[8]. Zhu, H. L., Cheung, S. W., & Yuk, T. I. Mechanically pattern reconfigurable antenna using metasurface. *IET Microwaves, Antennas & Propagation*, 9(12):1331–1336, 2015. DOI:10.1049/iet-map.2014.0676

[9]. A. H. Naqvi and S. Lim. A beam-steering antenna with a fluidically programmable metasurface. *IEEE Transactions on Antennas and Propagation*, 67(6):3704–3711, June 2019. DOI:10.1109/TAP.2019.2905690

[10]. L. Y. Ji, Y. J. Guo, P. Y. Qin, S.-X. Gong, and R. Mittra. A reconfigurable partially reflective surface (PRS) antenna for beam steering. *IEEE Transactions on Antennas and Propagation*, 63(6):2387–2395, June 2015.

[11]. Ji, L., Fu, S., Zhang, L., & Li, J. One-dimensional beam-steering Fabry–Perot cavity (FPC) antenna with a reconfigurable superstrate. *International Journal of Microwave and Wireless Technologies*, 12(3):233–239, 2019. DOI:10.1017/s1759078719001144

[12]. Ji, L., Guo, Y. J., Qin, P., Gong, S., & Mittra, R. A reconfigurable partially reflective surface (PRS) antenna for beam steering. *IEEE Transactions on Antennas and Propagation*, 63(6):2387–2395, 2015. DOI:10.1109/tap.2015.2412143